Progress In Electromagnetics Research M, Vol. 113, 115–128, 2022

A Tri-Band Miniaturized Antenna Using Fractal Defected Ground Structure for C/X and Ku-Band Applications

Kakani Suvarna[1, *], Nallagarla Ramamurthy[2], and Dupakuntla V. Vardhan[1]

Abstract—In this article, a miniaturized antenna with a Koch fractal defected ground structure (KFDGS) is proposed for C/X and Ku-band applications. The performance of an inset-fed lambda/2 patch antenna is examined using an iterated KFDGS etched on the ground plane. A conventional antenna operated at 16 GHz with a return loss of −34.31 dB is constructed, followed by a tri-band miniaturized antenna operating at 6.35, 9, and 13.05 GHz with a return loss of −22.41, −25.05, and −28.54 dB in order to achieve miniaturization of 60.31%, 43.75%, and 18.43%, respectively. An antenna is designed on a Roger RT Duroid substrate, fabricated, and tested with dimensions of $12 \times 14 \times 0.8\,\text{mm}^3$, and its impact on reduction in size performance has been evaluated with measured peak directivity and gain of 3.07 and 2.80 dBi at 6.35 GHz, 4.78 and 4.65 dBi at 9 GHz, and 7.73 and 7.76 dBi at 13.05 GHz, respectively. A good agreement is found between the measurements and simulations.

1. INTRODUCTION

Portable wireless devices necessitate the use of small wireless transceivers. An antenna is well established as part of an RF transceiver that takes up the most space. As a result, an RF designer's primary goal is to shrink the physical area of the antenna. Currently, the need for miniaturized antennas has grown tremendously to meet the demanding specifications of modern wireless communication systems. One of the most common techniques suggested for antenna miniaturization is space-filling curves, reactance compensation (specifically meandering/fractal antennas), and metamaterial-inspired designs, as presented by Fallahpour and Zoughi [1]. The successful miniaturization techniques for planar slot antennas using loop, wires, strips, and slits loading techniques were introduced [2–4]. By employing these techniques, the resonant frequency of the proposed antenna is reduced to electrically small antenna without influencing its characteristics. The term "electrically small antennas" refers to miniaturized antennas with $Ka \leq 1.0$, where $K = 2\pi/\lambda$ denotes the wave propagation vector, and "a" is the smallest sphere radius that encircles the antenna [5]. A resonant LC structure has been achieved by introducing efficient electrically-small antenna (EESA) design methodology [6]. The limitations of small antennas were outlined by Wheeler [7]. Radiating fields were defined as spherical modes by Chu [8]. Antennas loaded in slots, with loops at end, have been addressed by Haque and Parvez achieved a 29.51% reduction in resonant frequency without modifying the loaded slot length and reference antennas [9]. Jahani et al. described a helix-loaded miniaturized circular patch antenna that operates as mu negative (MNG) metamaterials and obtained a size reduction of 60% [10]. Khan et al. [11] made a survey on patch antenna miniaturization techniques including reshaping the antenna, material loading, folding, and shorting, introducing defects in the ground plane and slots. Various antenna miniaturization methods based on Single Ring Spilt Ring Resonator (SRR), Double Ring SRR, Complementary SRR (CSRR) , and fractals loaded were discussed [12–14]. Further, the wide-band antenna proposed by Sharma and Sharma [15] was based on a hybrid fractal slot with partial ground plane. For Vivaldi antenna

Received 23 March 2022, Accepted 17 June 2022, Scheduled 16 September 2022
* Corresponding author: Kakani Suvarna (kakanisuvarna@gmail.com).
[1] JNTUA, Ananthapuramu, India. [2] G. Pullaiah College of Engineering and Technology, Kurnool, India.

miniaturization, Ao et al. [16] designed a tapered patch using parasitic elements which is connected by a lumped resistor. Defected Ground Structure (DGS) has been used to miniaturize the patch and its array elements [17–21].

In this paper, two miniaturization methods are discussed, one with switching resonant frequency and the other with antenna size. Chu-limit is used to create a miniaturized Kochstar patch antenna with an iterated Koch fractal DGS loaded on it. The proposed antenna, with less compact size, exhibits measured peak directivity and gain 3.07 and 2.80 dBi at 6.35 GHz, 4.78 and 4.65 dBi at 9 GHz, and 7.73 and 7.76 dBi at 13.05 GHz, respectively, for C/X and Ku-band applications. In Table 1, DGS-based antennas are significantly larger at lower frequencies and have lower peak gains.

Table 1. Analysis of the DGS-based work suggested.

Ref.	**size (mm^2)**	**Miniaturization (%)**	**Switching resonance Frequency [GHz]**		**Application**	**Gain (dBi)**
			Before switch	**After switch**		
[17]	$0.28\lambda_0 * 0.28\lambda_0$	56.89	5.8	2.5	ISM	1.75
[18]	$0.2\lambda_0 * 0.22\lambda_0$	47.36	5.7	3	WiMAX	8.9
[19]	$0.1\lambda_0 * 1.25\lambda_0$	25.0	10	7.5	Arrays	4.12
[20]	$1.149\lambda_0 * 0.466\lambda_0$	57.77	5.8	2.45	ISM	2.14
[21]	$0.125\lambda_0 * 0.193\lambda_0$	53.6	5.8	2.69	Arrays	7.026
[27]	$0.25\lambda_0 * 0.243\lambda_0$	64.86	14.8	5.2	WLAN	3.32
Proposed	$0.26\lambda_0 * 0.31\lambda_0$	60.31.43.75 and 18.43	16	6.35, 9 and 13.05	Wireless data transmission	2.86, 4.65 and 7.76

2. MINIATURIZED ANTENNA DESIGN

In this paper, a tri-band miniaturized antenna is presented using Ansys HFSS and Keysight Advanced Design System (ADS). The top and bottom views of the proposed antenna configuration, which is excited by a lambda/2 feeder and has KFDGS etched on the ground plane, are shown in Figures 1(a) and 1(b). The mathematical Equations (1) and (2) represent the 50 ohm feeder length (L_f) and characteristic impedance (Z_0) of a microstrip line [22]. The substrate Roger RT Duroid, with a 0.8 mm height, dielectric permittivity of 2.2, and compact size of $0.26\lambda_0 * 0.31\lambda_0\,mm^2$, is used to resonate in the C/X and Ku-band at 6.35, 9, and 13.05 GHz, respectively.

$$L_f = \frac{L_{\lambda/2}}{\pi}\cos^{-1}\sqrt{\frac{50}{z_0}} \tag{1}$$

$$Z_0 = \frac{377}{\sqrt{\varepsilon_r\left(\frac{w}{h} + 1.393 + 0.667\ln\left(\frac{w_f}{h} + 1.444\right)\right)}} \tag{2}$$

Table 2 shows the optimized dimensions of proposed antenna. The length of line segment "l" of Koch curve is taken into account. The middle third part is removed, and this removed part is replaced with the length of two line segments $[\frac{1}{3}l]$, for a total of 4 line segments shown in Figure 1(c). This evolution reverses the same four line segments generated adjacent to the last iteration. In the next iteration, the following strategy has been implemented as shown in Figure 1(d). The second iteration resembles eagle flies stroke and is defined by using an iterative function system (IFS). Fractal curve has dimension in Equation (3), which relates D and $[\frac{1}{r}]^D = N$, where r is the scaling ratio = 1/3, and N is

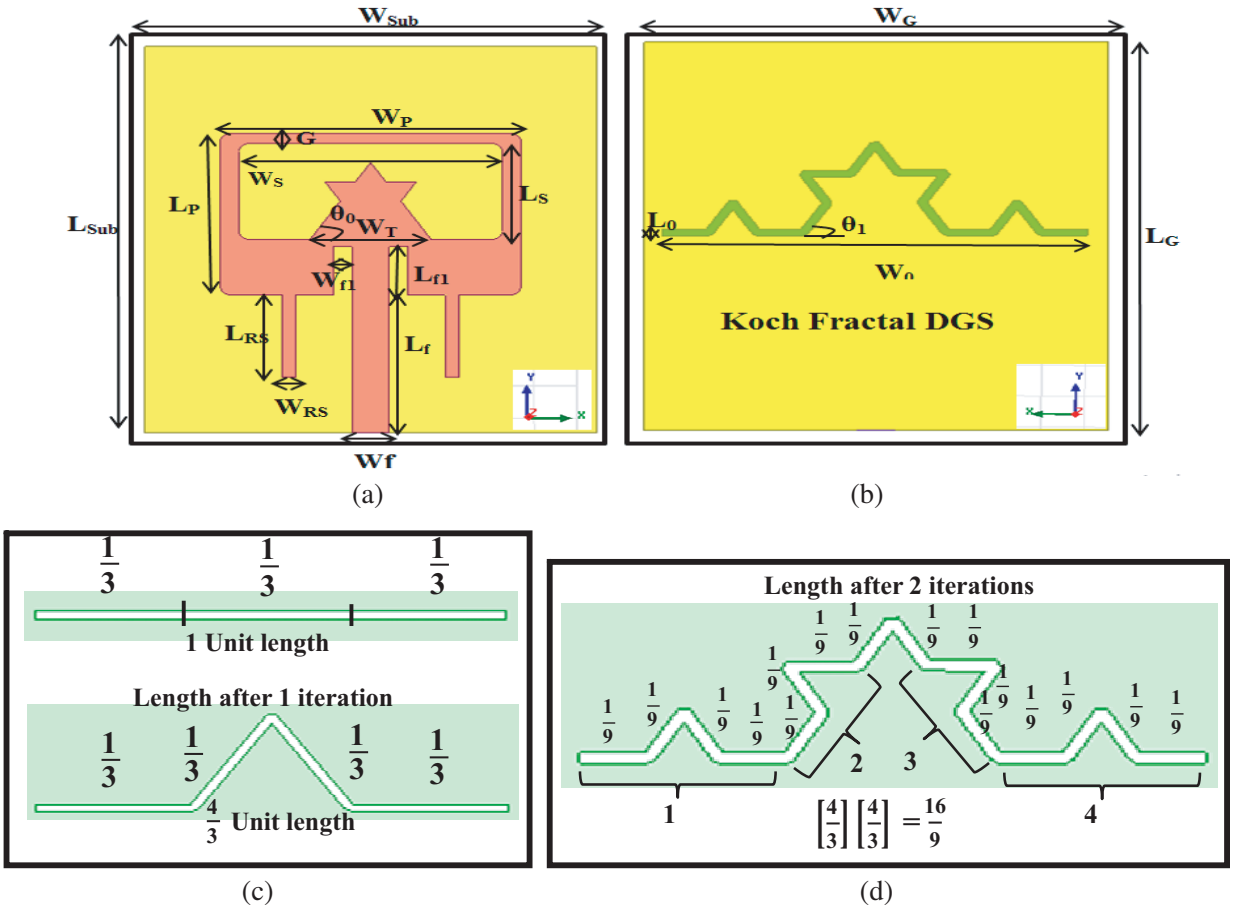

Figure 1. Geometry of the tri-band miniaturized antenna. (a) Top view. (b) Bottom view. (c) Koch fractal: Iteration 0, Iteration 1 and (d) Iteration 2.

Table 2. The optimized geometrical dimensions of the proposed antenna.

Parameters	Optimized Value [mm]	Parameters	Optimized Value [mm]
Ground width, W_G and substrate width, W_{Sub}	12	Width of Slot, W_s	7
Ground length, L_G and substrate length, L_{Sub}	14	Length of Slot, L_s	3.38
Patch length, L_p	8	Width of Rectangular Strip, W_{RS}	0.35
Patch width, W_p	5.86	Length of Rectangular Strip, L_{RS}	3
Substrate thickness, h	0.8	Triangle side w_T	3.23
Feed Width, W_f and Width of inset, W_{f1}	7	Koch star angle on patch θ_0 and ground θ_1	60°, 60°
Length of feed, L_f and Length of inset, L_{f1}	3.5	Width of KFDGS, W_0	11.4
Gap between L_p and L_s, G	0.36	Length of KFDGS, L_0	0.25

pieces that result from scaling. The iterative construction at every stage, $[\frac{1}{r}]^D = N[\frac{1}{1/3}]^D = 4$, $3^D = 4$, $\ln(3^D) = \ln(4)$, $D \cdot \ln(3) = \ln(4)$.

$$D = \frac{\ln[4]}{\ln[3]} = 1.262 \tag{3}$$

The fractal measurement is computed with self-similar property. Each point on the iteration has a similar effect on the overall picture. The HausDorff-Besicovitch equation-Koch curve, in particular, represents N by 4 and r by 3 from (4) to (7). The iterative function system (IFS), introduced in [26], is a universal method for generating a wide range of fractal structures. It is based on a series of affine transformations W, defined by

$$W_1(J,K) = \left[\frac{1}{3}(J); \frac{1}{3}(K)\right] \tag{4}$$

$$W_2(J,K) = \left[\frac{1}{6}(J); \frac{\sqrt{3}}{6}(K) + \frac{1}{3}; \frac{\sqrt{3}}{6}(J) + \frac{1}{6}(K)\right] \tag{5}$$

$$W_3(J,K) = \left[\frac{1}{6}(J); \frac{\sqrt{3}}{6}(K) + \frac{1}{2}; \frac{\sqrt{3}}{6}(J) + \frac{1}{6}(K) + \frac{\sqrt{3}}{6}\right] \tag{6}$$

$$W_4(J,K) = \left[\frac{1}{3}(J) + \frac{2}{3}; \frac{1}{3}(K)\right] \tag{7}$$

where w_1, w_2, w_3, and w_4 are as a system of linear affine transformations with respect to the axis of coordinating system J and k.

The design procedure has been discussed in greater detail below. Figure 2 depicts the steps taken to complete the tri-band miniaturized Koch star patch antenna using KFDGS and fabricated prototype. Initially, a rectangle-shaped radiator operates in Ku-band at 16 GHz along with gain of 8.10 dBi and

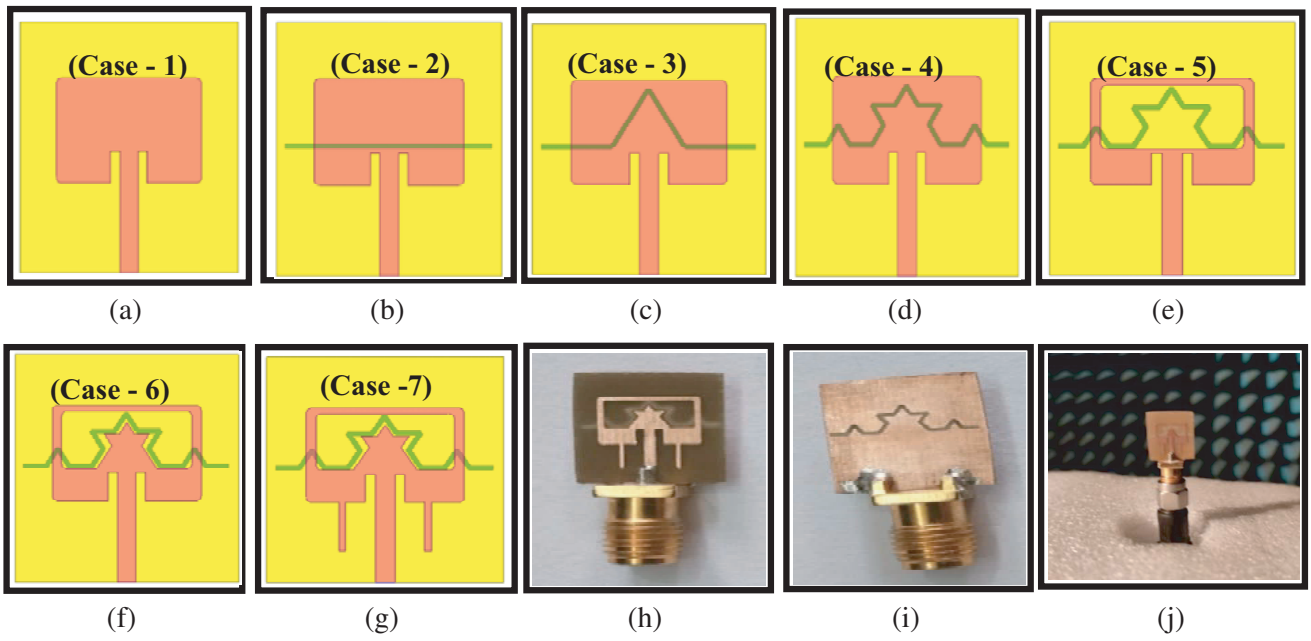

Figure 2. The steps involved in creating a tri-band miniaturized antenna. (a) Inset Fed conventional antenna, (b) First iteration, (c) Second iteration, (d) Third iterations of KFDGS, (e) KFDGS on the ground plane and rectangular slot is etched on the patch of conventional antenna, (f) Koch star is created in the slot area of conventional antenna, (g) Koch star and two rectangular strips are added to patch, (h) Top view, (i) Flipside view and (j) Measurement chamber of fabricated prototype.

impedance bandwidth of 4.86%, as shown in case-1 of Figure 2(a). The antenna is modified by etching a Koch fractal defected structure on ground plane. This etching is carried out for shifting the frequency to lower band. As a result, the antenna is miniaturized. The idea under antenna miniaturization is simply to switch the frequency from the Ku band (f_1) to the C/X and Ku-bands (f_2) without altering the dimensions of the antenna. Equation (8) reflects the miniaturization factor [23, 24].

$$M = \frac{f_2}{f_1} \tag{8}$$

The DGS is characterized by periodic or non-periodic structures that are removed from the ground plane, require little area, and are simple to design. When DGS is realized with a microstrip antenna, current distribution is disrupted due to the etched defect in the ground. The surface current flow and impedance are influenced by the values of line inductance and capacitance of the antenna, which are formed due to changes in the current distribution [20]. As a result, the resonance frequency is shifted from 16 to 8.25 GHz by increasing the antenna electrical length (βl). After the introduction of the first iteration of KFDGS on the ground plane, the gain is reduced to 4.83 dBi and the impedance bandwidth to 8.39% at the operating frequency of 8.25 GHz, as shown in case-2 of Figure 2(b). Later, it is changed by etching the second iteration of KFDGS on the ground, resulting in a 3.81 dBi gain decrement, and a resonant frequency shifts to 7.45 GHz and impedance bandwidth to 5.85%, as shown in case-3 of Figure 2(c). By modifying the design structure for the third iterations of KFDGS on the ground plane, the antenna is operated at a lower frequency band, resulting in antenna miniaturization. Case-4 in Figure 2(d) shows that at 6.65 GHz, the gain is improved to 4.57 dBi with an impedance bandwidth of 5.26%. Using rectangular slot geometry on the patch, current is disrupted throughout the patch, and due to this the resonance frequency is shifted by increasing the electrical length (βl) antenna, which affects capacitance and inductance values, resulting in an increase in realized gain and a decrease in resonant frequency. As depicted in case-5 in Figure 2(e), the gain is 6.10 dBi at a frequency of 6.65 GHz with an impedance bandwidth of 4.60%. To achieve dual bands, a Koch star is formed with the spike apex angles of 60° and 120°, in the rectangular slot area of a conventional antenna patch with simulated reflection coefficients (S_{11}) of −30.98 and −38.59. Here, the first band resonates at 6.65 GHz with changing the position of KFDGS, and a Koch star is optimized to get the second band at 9.65 GHz for desired frequencies with impedance bandwidth of 4.69% and 1.74%, respectively, in case-6 of Figure 2(f). Finally, in case-7 of Figure 2(g), a miniaturized Koch star with two rectangular strips has been added to a conventional patch antenna which operates in the C/X and Ku-bands at 6.35, 9 and 13.05 GHz, respectively. The characteristics of miniaturized antenna for different stages are compared in Table 3, from case-1 to case-7, respectively.

Table 3. Characteristics of miniaturized antenna for different stages.

parameter	Case-1	Case-2	Case-3	Case-4	Case-5	Case-6	Case-7
Resonant freq. (GHz)	16	8.1	7.45	6.65	6.55	6.65, 9.65	6.35, 9 and 13.05
Ka and Q_{chu}	2.34, 0.49	1.18, 1.45	1.09, 1.68	0.97, 2.09	0.97, 2.09	0.97, 2.09, 1.41, 1.05,	0.93, 2.28 and 1.33, 1.17, 1.99 and 0.628
Gain (dBi)	8.10	4.82	3.81	4.57	6.10	2.91,3.99	2.80, 4.65 and 7.76
Bandwidth (GHz)	0.8	0.71	0.45	0.36	0.31	0.32, 0.17	0.22, 0.13, and 0.28
Directivity (dBi)	8.10	4.92	4.01	4.73	6.28	2.55, 4.54	3.07, 4.78 and 7.73
Efficiency (%)	95.8	60.1	63.4	64.6	81.3	78.2, 82.5	70, 77.5 and 82.7
E-plane (dB) $\theta = 0°$, $\phi = 0°$	7.69	3.28	−13.29	0.854	5.28	6.87	2.67
H-plane (dB) $\theta = 90°$, $\phi = 90°$	−5.79	−4.21	−1.49	−1.54	−3.74	−3.78	−1.55
V_{swr}	1.01	1.04	1.11	1.03	1.09	1.06, 1.02	1.18, 1.2 and 1.03

A tri-band miniaturized Koch star patch antenna that meets the Chu-limit specified in Equation (9) is designed to have good peak gain and return loss characteristics at operating frequencies.

$$Chu_Q = \frac{1}{ka} + \frac{1}{(ka)^3} \tag{9}$$

The antenna structure inside the sphere with radius "a" and source distribution are related by the mathematical method proposed by McLean [5]. The tri-band miniaturized antenna Chu-limit is measured using a sphere with a radius of 7 mm. In antennas, Q is known as half power bandwidth, namely, $Q = 1/BW$. Table 3 lists information about the characteristics of each design. Figures 3(a) and (b) show the lumped equivalent circuit and layout model for the proposed tri-band miniaturized antenna. A good way to solve a problem is to include a lumped element in the equivalent circuit model using Keysight Advanced Design System (ADS) for each part of the antenna. Correct modeling of the antenna is required to determine the correct value of elements. An open-ended transmission line is similar to the microstrip patch antenna in general. Following are the C, L, and R values corresponding to the frequency of the microstrip patch antenna. The following formulas ((10) to (13)) can be used to calculate the parameters of an equivalent circuit (R, L, and C) and to determine the quality factor of the resonator, where X_0 is the feed point location.

$$C = \frac{\varepsilon_0 \varepsilon_r LW}{2h} \cos^2 \frac{\pi X_0}{L} \tag{10}$$

$$L = \frac{1}{C\omega_r^2} \tag{11}$$

$$R = \frac{Q}{C\omega_r^2} \tag{12}$$

$$\text{Quality Factor}, Q = \frac{c\sqrt{\varepsilon_e}}{4fh} \tag{13}$$

The values of L_F and C_F in the equivalent circuit of the microstrip line feed are given by Equations (14) and (15)

$$L_F = 100h\left(4\sqrt{\frac{w_f}{h-4.21}}\right) \text{(nH)} \tag{14}$$

$$C_F = W_f[(9.5\varepsilon_r + 1.25)\frac{w_f}{h} + 5.2\varepsilon_r + 7] \text{(pF)} \tag{15}$$

The extracted and optimized parameter values of lumped equivalent circuit are $L_F = 0.01$ nH, $C_F = 1.7$ pF $R_P = 123.55\,\Omega$, $L_P = 64$ pH, $C_P = 2$ pF, $L_{strip} = 0.166$ nH, $C_{strip} = 0.99$ pF, $L_{slot} = 0.41$ nH, $C_{slot} = 0.895$ pF, $R_{dgs} = 80$ ohms, $L_{dgs} = 94.501$ pH, and $C_{dgs} = 10.39$ pF. Using $50\,\Omega$ load impedance, antennas can be used to achieve perfect matching in communication systems. Several nearby resonances can be combined to switch frequency in a tri-band miniaturized antenna, and parallel RLC tank circuits arranged in series can correspond to each resonance as shown in Figure 3(a).

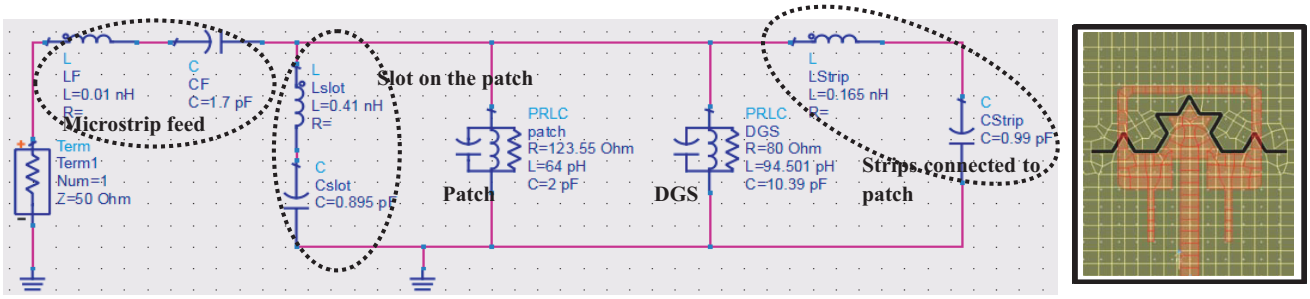

(a) (b)

Figure 3. (a) Equivalent circuit model, (b) Layout for tri-band miniaturized Koch star patch antenna using KFDGS using ADS.

C_F and L_F are represented as series in the equivalent circuit by microstrip feed static capacitance and inductance, respectively. C_{strip} and L_{strip} are capacitance and inductance in relation to the size of the strips connected to the patch, whereas C_{slot} and L_{slot} are capacitance and inductance with respect to the rectangular slots within the patch. The proposed equivalent circuit model is discussed in terms of the rectangular slot element (C_{slot} and L_{slot}) and real radiation resistance (R_r) of the antenna element. The total input admittance of the equivalent circuit model is given by:

$$Y_{in} = \frac{1}{R_r} + \frac{1}{j\omega L_{slot}} + j\omega C_{slot} \tag{16}$$

A parallel slot resonator with R-L-C, C_{slot} and L_{slot} inductor and capacitor values has been studied for the effect on bandwidth and resonance frequencies. The resonance frequency can be expressed as [28]:

$$W_0 = \frac{1}{\sqrt{L_{slot}C_{slot}}} \quad \text{and} \quad \omega = \omega + \Delta\omega \tag{17}$$

Simplifying Equation (8):

$$Y_{in} = \frac{1}{R_r} + \frac{j}{\omega L_{slot}} + \omega^2 \cdot C_{slot}L_{slot} - 1 \tag{18}$$

From Equations (17) and (18):

$$\begin{aligned} Y_{in} &= \frac{1}{R_r} + \frac{j}{\omega L_{slot}} + (\Delta\omega^2 + 2\omega_0 \cdot \Delta\omega)C_{slot}L_{slot} \\ Y_{in} &\sim \frac{1}{R_r} + j\Delta\omega L_{slot} \cdot 2C_{slot} \end{aligned} \tag{19}$$

Y_{in} is the input admittance of a parallel $2C_{slot}$ and R_r circuit operating near zero GHz. As a result, -3 dB bandwidth of the equivalent R-L-C resonance circuit almost doubles -3 dB bandwidth of the parallel R_r and $2C$s circuit, as given by:

$$\text{Bandwidth (BW)} = \frac{2}{R_r 2C_{slot}} = \frac{1}{R_r C_{slot}} \tag{20}$$

Hence, it can be concluded from the above analysis that the bandwidth (BW) and resonance frequencies can be shifted by increasing the length of the slot, which is similar to increasing the value of the capacitor. However, by increasing the width of the slot, the inductance value decreases.

3. RESULTS AND DISCUSSION

The response of the circuit model is compared to the response of the HFSS simulation, as shown in Figure 4(a). This result shows that the two graphs agree well with each other. Both responses nearly have return losses of -22.41, -25.05, and -28.54 dB at the resonant frequencies 6.35, 9, and 13.05 GHz. The measured and simulated return losses are plotted with good agreement in Figure 4(b). The simulated return loss (S_{11}) is involved in developing a tri-band miniaturized antenna and is shown in Figure 4(c). Finally Figure 4(d) depicts a parametric analysis of the different slot sizes of KFDGS (iteration 0). In iteration 0, the rectangular slot size varies by 0.5 mm, due to the presence of KFDGS. By doing so, it allows the first resonances (from right to left) to switch to a lower frequency. The return loss of the tri-band miniaturized antenna is measured using an Agilent N5247A VNA.

Figure 5 shows the simulated and measured radiations in the (phi = 0°) E plane and H plane (phi = 90°) of a tri-band miniaturized Koch star patch antenna at operating frequencies, showing only semi-dumbbell-shaped radiation in the E plane similar to the dipole element at 6.35, 9, and 13.05 GHz. A quasi-omnidirectional pattern is observed in the H plane at tri-bands. A perfect correlation is also observed between the simulated and measured results. Figure 6(a) depicts the current distribution close to the feed line at 6.35 GHz, in C band. Figure 6(b) shows how the edges of the iterated Koch DGS fractal interacts with the current at 9.0 GHz in X band. As shown in Figure 6(c), the maximum current density in the tri-band KFDGS loaded miniaturized Koch star patch antenna is realistic for Ku band frequency at 13.05 GHz. Figure 7(a) shows measured peak directivity and gain of a conventional antenna as 8.26 and 8.74 dBi at 16 GHz, respectively. The tri-band miniaturized antenna using KFDGS

is measured peak directivity and gain given as 3.07 and 2.80 dBi at 6.35 GHz, 4.78 and 4.65 dBi at 9 GHz, and 7.73 and 7.76 dBi at 13.05 GHz, respectively, conveyed in Figure 7(b). The fidelity factor is a major component in the time domain analysis for signifying the antenna's characteristics. In wireless communication, a strong correlation is found between a transmitted and a received signal for reducing losses in the modulated signal. Figure 7(c) depicts two identical antennas mounted 30 cm apart in a side-by-side configuration in order to determine the pulse characteristics of the proposed antenna miniaturization.

Figures 7(d), (e), and (f) describe the experimental and simulated input and received signal attributes of a time domain method. The correlation of fidelity factor is calculated [25], and the

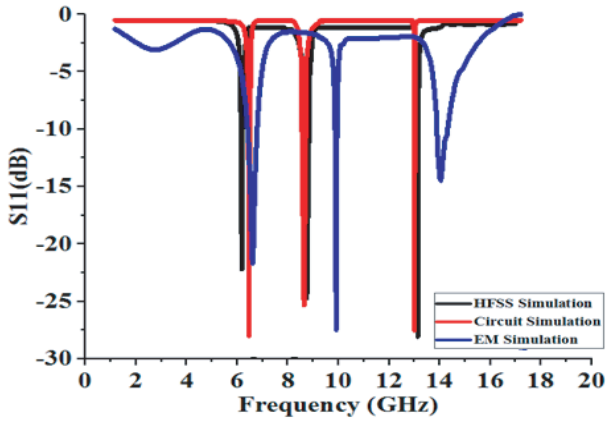

(a)

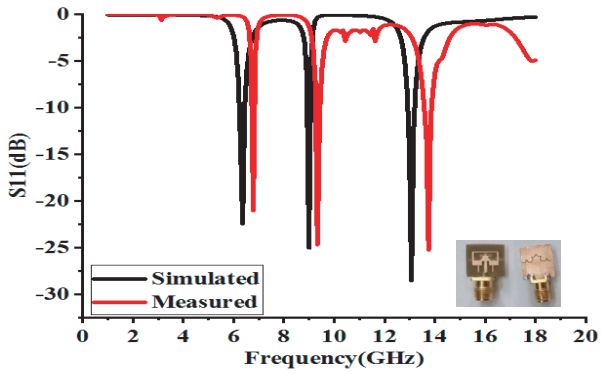

(b)

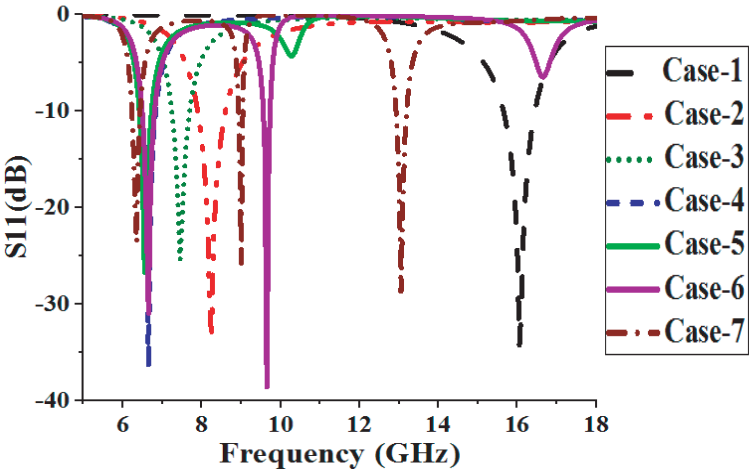

(c)

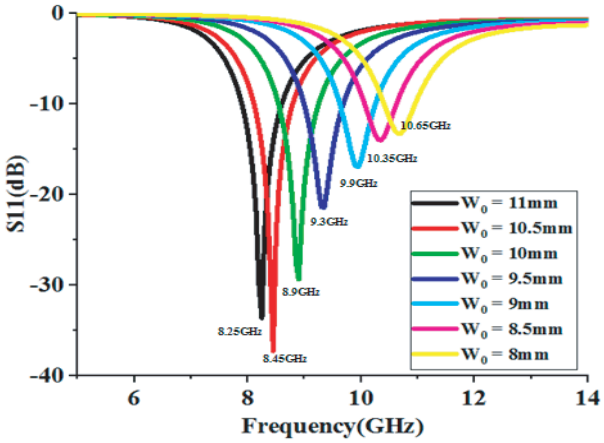

(d)

Figure 4. Return loss (a) comparison of simulated tri-band miniaturized antenna using HFSS, circuit simulation and EM simulation, (b) Measured results, (c)) Simulation process involved in developing a tri-band miniaturized antenna. (d) A simulation of KFDGS (iteration 0) with a different slot size 'W_0'.

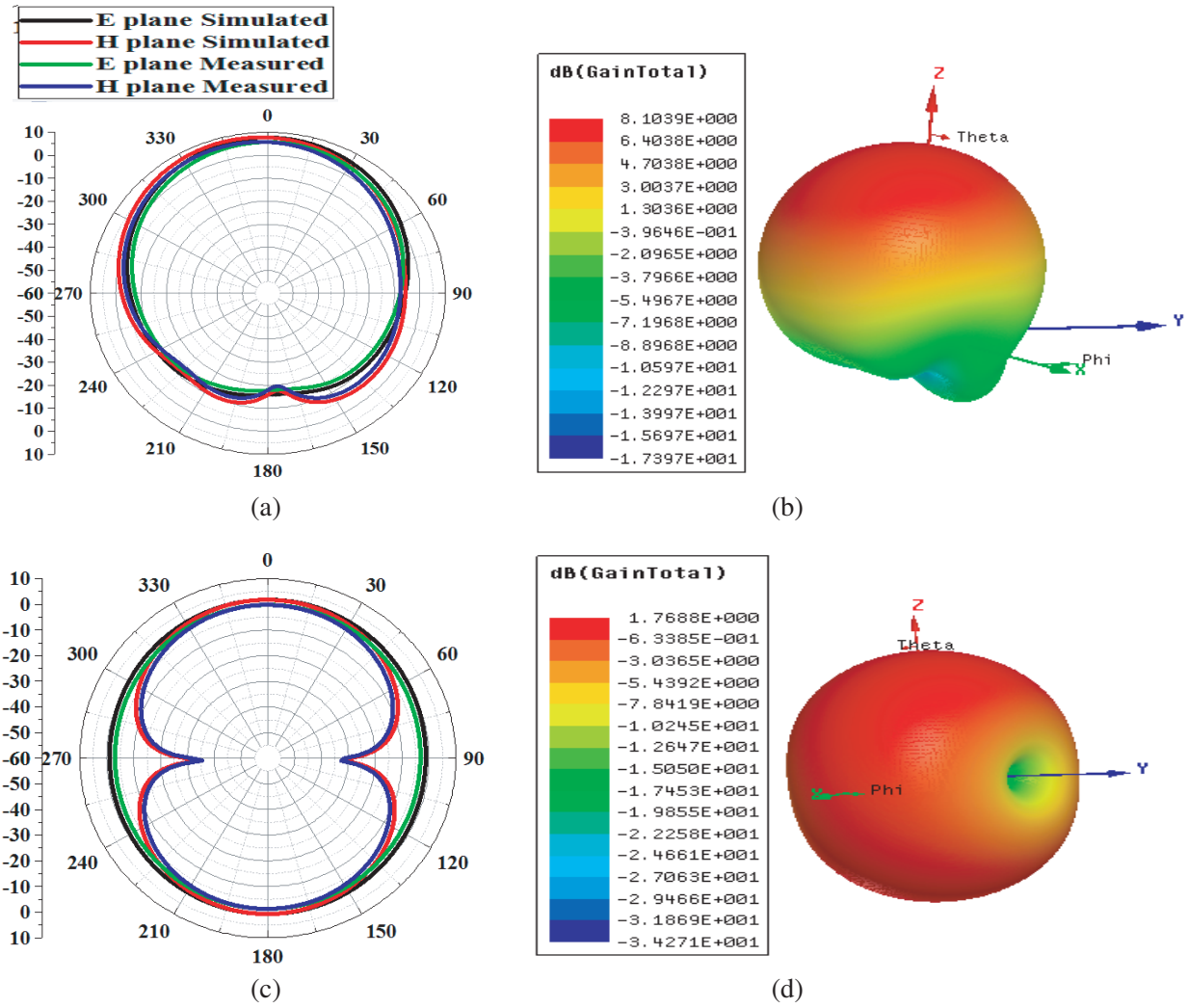

(a) (b)

(c) (d)

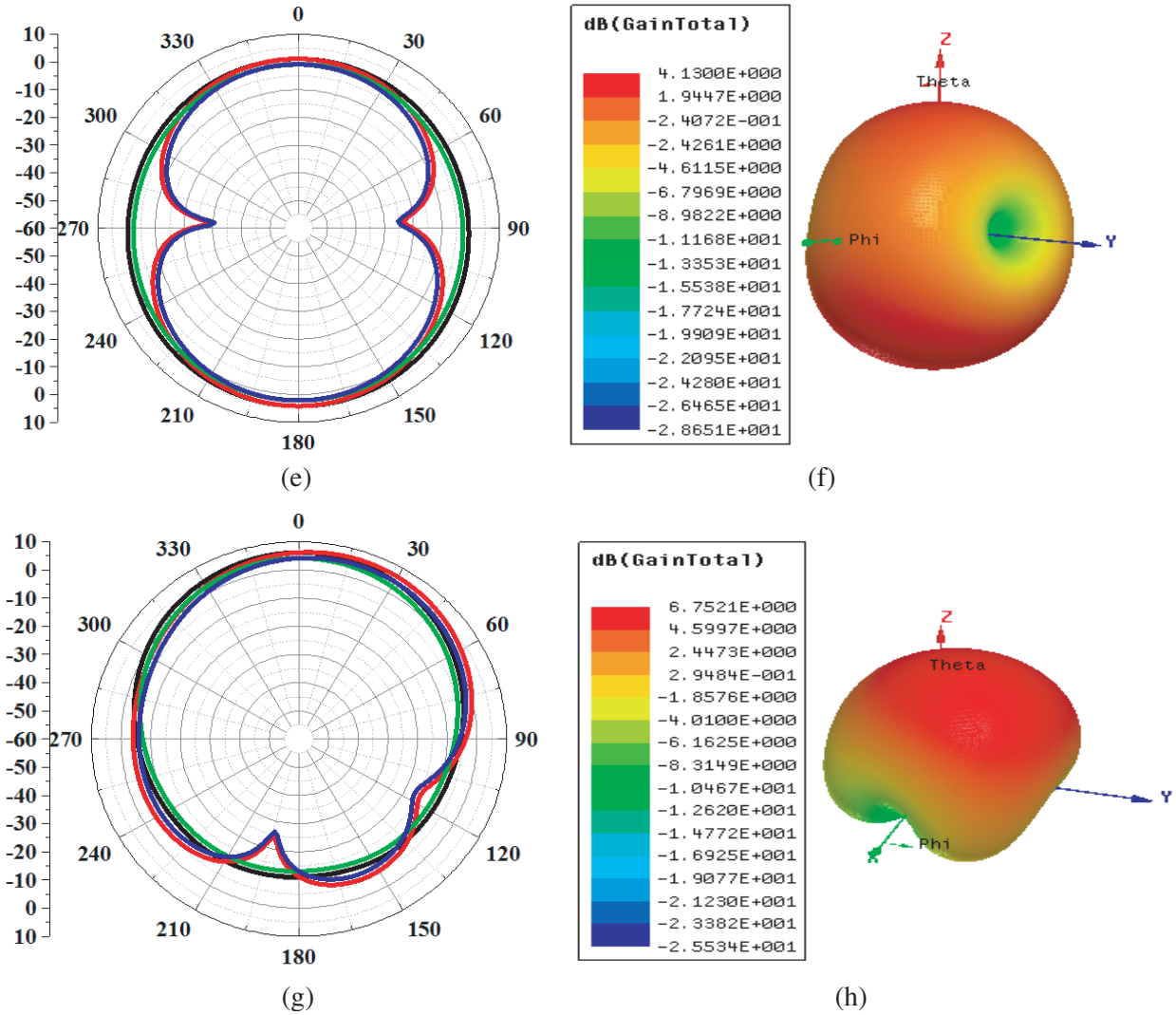

Figure 5. Measured, simulated radiation pattern results and 3D gain plot, (a) and (b) for Conventional antenna at 16 GHz, (c) and (d) at 6.35 GHz, (e) and (f) at 9 GHz, (g) and (h) at 13.05 GHz for tri-band miniaturized antenna.

similarity between the input and received signals is calculated using Equation (21), where $a(t)$ and $b(t)$ are the transmitted and received signals, respectively. The obtained fidelity factor is 84% for the input and transmitted signal, 80% for the transmitted to receive signal, and 78% for the experimental results. The oval shape in Figure 7 indicates that gain increases with frequency. Table 4 compares the proposed miniaturized tri-band antenna to previously published studies.

$$F = \max_{\tau} \left| \frac{\int_{-\infty}^{+\infty} a\,(t)\, b\,(t-\tau)\, dt}{\sqrt{\int_{-\infty}^{+\infty} a(t)^2 dt \int_{-\infty}^{+\infty} b(t)^2 dt}} \right| \tag{21}$$

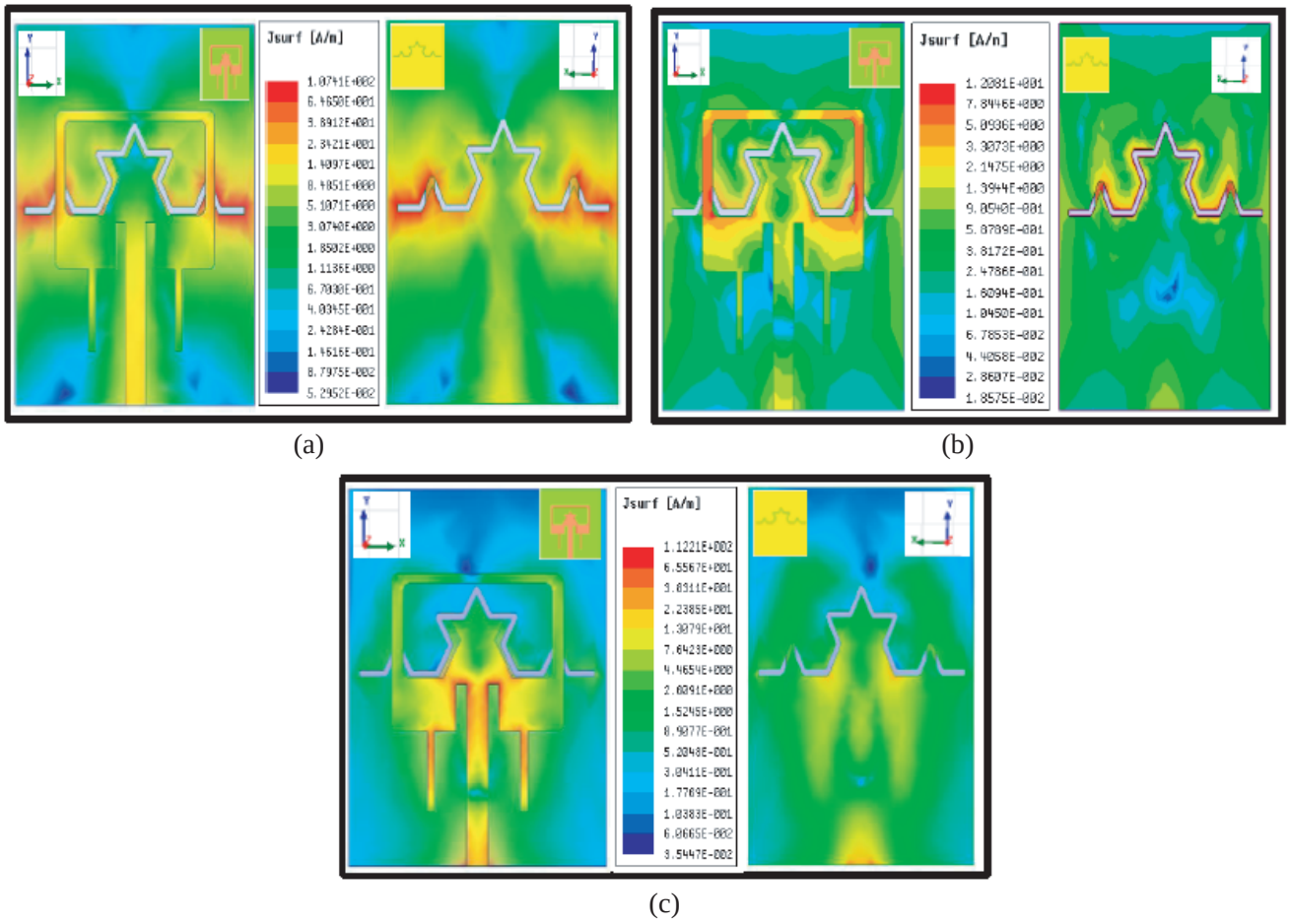

Figure 6. Surface current distributions of tri-band miniaturized antenna using KFDGS. (a) 6.35 GHz, (b) 9 GHz, (c) 13.05 GHz.

Table 4. Comparison of different existing miniaturization-based literature by way of tri-band miniaturized proposed antenna.

Ref.	Type of loading	size (mm^2)	Switching Resonance Frequency [GHz] enclosed by antenna		Miniaturization (%)	working bands	Gain (dBi)	Fidelity factor
			Before switch	After switch				
[2]	Loop	$0.561\lambda_0 * 0.561\lambda_0$	2.01	1.53	23.88	Single	−3.4	No
[3]	Wire	$0.812\lambda_0 * 0.812\lambda_0$	3.26	2.03	28.83	Single	NA	No
[4]	Slit, strip	$1.16\lambda_0 * 1.16\lambda_0$	3.26	2.32	37.73	Single	0.5 dB	No
[13]	Fractal EBG and SRR	$0.3\lambda_0 * 0.3\lambda_0$	4.2	2.5	40.47	Single	3.77	No
[14]	HRI metamaterial	$0.5\lambda_0 * 0.5\lambda_0$	4.225	2.5	40.8	Single	−1.1	No
Proposed	Koch Fractal DGS	$0.26\lambda_0 * 0.31\lambda_0$	16	6.35, 9, and 13.05	60.31, 43.75, and 18.43	Tri	2.80, 4.65, and 7.76	Yes

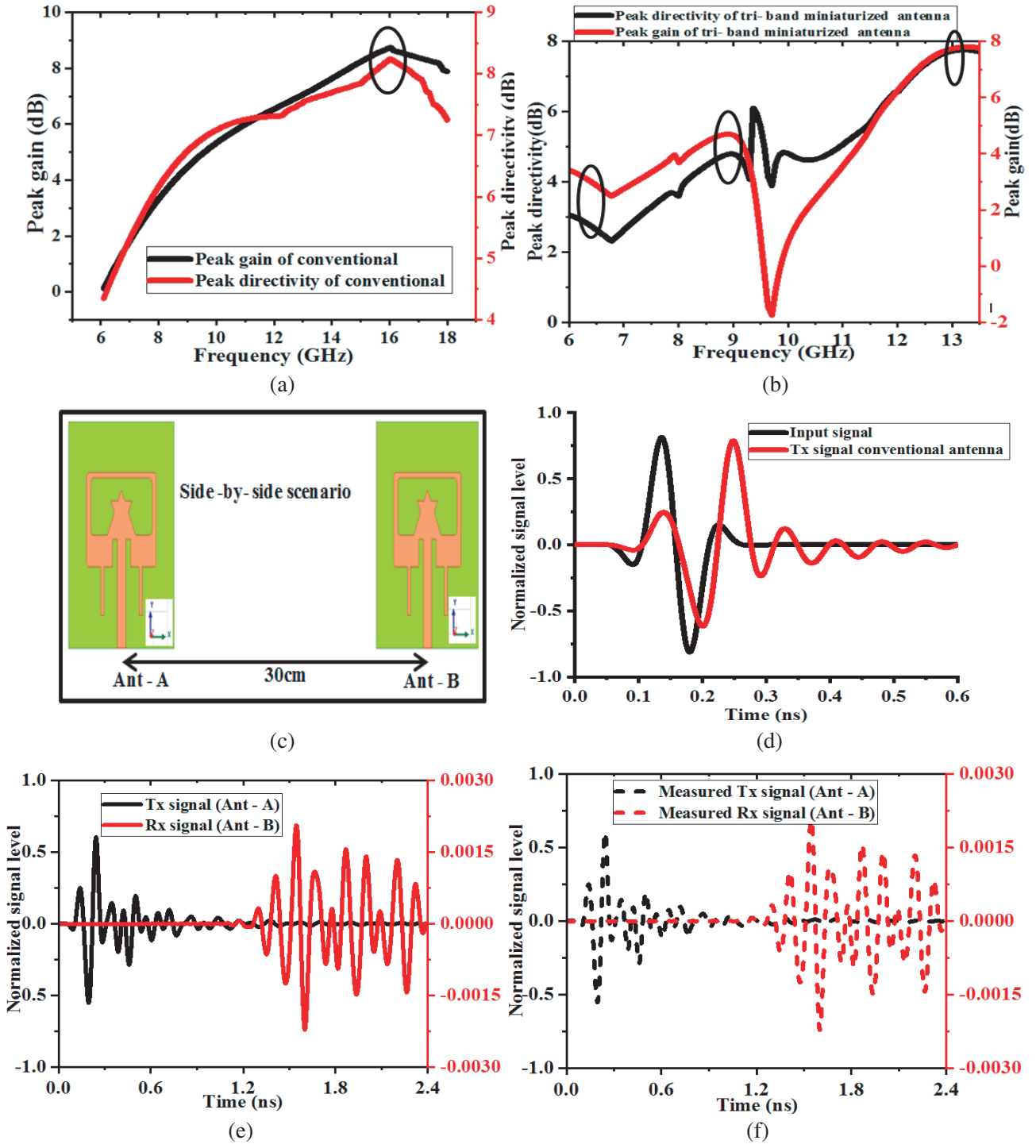

Figure 7. Measured results of peak gain and peak directivity vs frequency of (a) conventional antenna, (b) tri-band antenna, (c) side by side scenario for time domain performance, (d) the normalized signal level — input and transmit signal, (e) simulated transmit and receive signal and (f) measured transmit and receive signal.

4. CONCLUSION

This article presents a Koch fractal defected ground structure (KFDGS) loaded miniaturized Koch star patch antenna for C, X, and Ku band applications, which operates at 6.35, 9, and 13.05 GHz, has return loss (S_{11}) of -22.41, -25.05, and -28.54 dB, respectively, and achieves miniaturization of 60.31%, 43.75%, and 18.43%. The antenna is $12 \times 14 \times 0.8\,\text{mm}^3$ in size and is designed on a Roger RT Duroid. It operates in tri-bands with acceptable peak directivity of 3.07, 4.78, and 7.73 dBi, respectively. At 6.75 GHz, a KFDGS achieves $Ka \leq 1$. The time domain analysis has been implemented in a side-to-side layout to determine the fidelity factor of the proposed antenna. The bandwidths of 0.22, 0.13, and 0.28 GHz are achieved at bands ranging from 6.22 to 6.44 GHz, 8.92 to 9.05 GHz, and 12.92 to 13.20 GHz, respectively, and in terms of percentages they are 3.46, 1.44, and 2.14 percent.

REFERENCES

1. Fallahpour, M. and R. Zoughi, "Antenna miniaturization techniques: A review of topology- and material-based methods," *IEEE Antennas and Propagation Magazine*, Vol. 60, No. 1, 38–50, Feb. 2018.
2. Ghosh, B., S. M. Haque, D. Mitra, and S. Ghosh, "A loop loading technique for the miniaturization of non-planar and planar antennas," *IEEE Transactions on Antennas and Propagation*, Vol. 58, No. 6, 2116–2121, Jun. 2010.
3. Ghosh, B., S. K. Moinul Haque, and N. Rao Yenduri, "Miniaturization of slot antennas using wire loading," *IEEE Antennas and Wireless Propagation Letters*, Vol. 12, 488–491, 2013.
4. Ghosh, B., S. M. Haque, and D. Mitra, "Miniaturization of slot antennas using slit and strip loading," *IEEE Transactions on Antennas and Propagation*, Vol. 59, No. 10, 3922–3927, Oct. 2011.
5. McLean, J. S., "A re-examination of the fundamental limits on the radiation Q of electrically small antennas," *IEEE Transactions on Antennas and Propagation*, Vol. 44, 672–676, May 1996.
6. Erentok, A. and R. W. Ziolkowski, "Metamaterial-inspired efficient electrically small antennas," *IEEE Transactions on Antennas and Propagation*, Vol. 56, 691–707, Mar. 2008.
7. Wheeler, H. A., "Fundamental limitations of small antennas," *Proceedings of the I.R.E*, Vol. 35, 1479–1484, Dec. 1947.
8. Chu, L. J., "Physical limitations of omnidirectional antennas," *J. Applied Physics*, Vol. 19, 1163–1175, Dec. 1948.
9. Haque, S. K. M. and K. M. Parvez, "Slot antenna miniaturization using slit, strip, and loop loading techniques," *IEEE Transactions on Antennas and Propagation*, Vol. 65, No. 5, 2215–2221, May 2017.
10. Jahani, S., M. J. Rashed, and M. Shahabadi, "Miniaturization of circular patch antennas using MNG metamaterials," *IEEE Transactions on Antennas and Propagation*, Vol. 9, 1194–1196, 2010.
11. Khan, M. U., S. S. Mohammad, and R. Mittra, "Microstrip patch antenna miniaturization techniques: A review," *IET Microwave Antennas and Propagation*, Vol. 9, No. 9, 913–922, 2015.
12. Shrestha, S., S. R. Lee, and D. Y. Choi, "A new fractal-based miniaturized dual band patch antenna for RF energy harvesting," *International Journal of Antennas and Propagation*, 1–9, 2014.
13. Sedghi, M. S., M. Naser-Moghadasi, and F. B. Zarrabi, "Microstrip antenna miniaturization with fractal EBG and SRR loads for linear and circular polarizations," *International Journal of Microwave and Wireless Technologies*, Vol. 9, No. 4, 891–901, May 2017.
14. Bharath Reddy, G., M. H. Adhithya, and D. Sriram Kumar, "Miniaturization of microstrip slot antenna using high refractive index metamaterial based on single ring split ring resonator," *Progress In Electromagnetics Research Letters*, Vol. 93, 115–122, 2020.
15. Sharma, N. and V. Sharma, "A design of Microstrip Patch Antenna using hybrid fractal slot for wideband applications," *Ain Shams Engineering Journal*, Vol. 9, No. 4, 2491–2497, Dec. 2018.
16. Ao, J., J. Huang, W. Wu, and N. Yuan, "A miniaturized Vivaldi antenna by loading with parasitic patch and lumped resistor," *AEU: International Journal of Electronics and Communications*, Vol. 81, 158–162, Nov. 2017.

17. Er Rebyiy, R., J. Zbitou, M. Latrach, A. Tajmouati, A. Errkik, L. E. L. Abdellaoui, "New miniature planar microstrip antenna using DGS for ISM applications," *Telkomnika*, Vol. 15, No. 3, 1149–1154, Sep. 2017.
18. Oulhaj, O., N. A. Touhami, M. Aghoutane, and A. Tazon, "A miniature microstrip patch antenna array with defected ground structure," *International Journal of Microwave and Optical Technology*, Vol. 11, No. 1, 32–39, Jan. 2016.
19. Elftouh, H., N. A. Touhami, and M. Aghoutane, "Miniaturized microstrip patch antenna with spiral defected microstrip structure," *Progress In Electromagnetics Research Letters*, Vol. 53, 37–44, 2015.
20. Elftouh, H., N. A. Touhami, M. Aghoutane, S. El Amrani, A. Tazon, and M. Boussouis, "Miniaturized microstrip patch antenna with defected ground structure," *Progress In Electromagnetics Research C*, Vol. 55, 25–33, 2014.
21. Ghaloua, A., J. Zbitou, L. El Abdellaoui, M. Latrach, A. Tajmouati, and A. Errkik, "A novel configuration of a miniature printed antenna array based on defected ground structure," *International Journal of Intelligent Engineering and Systems*, Vol. 12, No. 1, 211–220, 2019.
22. Huang, Y. and K. Boyle, *Antennas from Theory to Practice*, John Wiley & Sons Ltd, UK, 2008.
23. Volakis, J. L., C.-C. Chen, and K. Fujimoto, *Small Antennas: Miniaturization Techniques and Applications*, McGraw-Hill, New York, NY, 2010.
24. Hansen, R. C. and R. E. Collin, *Small Antenna Handbook*, Wiley, Hoboken, NJ, 2011.
25. Quintero, G., J. F. Zurcher, and A. K. Skrivervik, "System fidelity factor: A new method for comparing antennas," *IEEE Transactions on Antennas and Propagation*, Vol. 59, No. 7, 2502–2512, 2011.
26. Elavarasi, C. and T. Shanmuganantham, "Multiband SRR loaded Koch star fractal antenna," *Alexandria Engineering Journal*, Vol. 57, No. 3, 1549, 2018.
27. Swetha, A. and K. Rama Naidu, "Miniaturized planar antenna with enhanced gain characteristics for 5.2 GHz WLAN application," *International Journal of Electronics*, Vol. 108, No. 12, 2137–2154, 2021.
28. Meena, M. L., M. Kumar, G. Parmar, and R. S. Meena, "Design analysis and modeling of UWB antenna with elliptical slotted ground structure for applications in C- & X-bands," *Progress In Electromagnetics Research C*, Vol. 63, 193–207, 2016.